Time-resolved energy spectrum measurement of a linear induction accelerator with the magnetic analyzer [*]

WANG Yuan(王远)   JIANG Xiao-Guo(江孝国)[1)]   YANG Guo-Jun(杨国君)   CHEN Si-Fu(陈思富)

ZHANG Zhuo(张卓)   WEI Tao(魏涛)   LI Jin(李劲)

Institute of Fluid Physics, China Academy of Engineering Physics, P.O.Box 919-106, Mianyang 621900, China

Abstract: We recently set up a time-resolved optical beam diagnostic system. Using this system, we measured the high current electron beam energy in the accelerator under construction. This paper introduces the principle of the diagnostic system, describes the setup, and shows the results. A bending beam line was designed using an existing magnetic analyzer with a 300 mm-bending radius and a 60° bending angle at hard-edge approximation. Calculations show that the magnitude of the beam energy is about 18 MeV, and the energy spread is within 2%. Our results agree well with the initial estimates deduced from the diode voltage approach.

Key words: LIA (linear induction accelerator), time-resolved optical beam diagnostic system, magnetic analyzer, energy spectrum

PACS: 78, 29.25.Dz, 29.27.Ac, 41.85.Ar   **DOI:** 10.1088/1674-1137/39/1/017004

1   Introduction

In recent years, the development of the technology of linear induction accelerators (LIAs), either in energy, beam current, or pulse form, has raised increasingly rigorous requirements on the resolving power and dynamic range of the beam testing system. In this context, we set up a time-resolved optical diagnostic system especially for the measurement of the beam energy spectrum. This paper describes the design, set up and testing of the diagnostic system [1].

The beam energy can be calculated by measuring the beam orbit through a bending element on the beam line. This system appears to have several important advantages over the traditional systems and is showing promise as an advanced diagnostic of charged particle beams. Two of the main advantages of this system are its time-resolving capability and the wide dynamic range. The synchronization precision is about 1 ns and the time-resolved capability of the system can reach 2 ns. A sampling frequency of 12–20 point/mm helps to obtain any minute changes throughout the duration of the pulse [2–4].

2   Principles

2.1   The momentum dispersion

For a particle moving at a uniform velocity, if we apply a uniform magnetic field perpendicular to its orbit, the Lorentz force is [5]

$$F = qvB, \tag{1}$$

where F is the force on the particle, q is the particle charge, v is the scalar velocity, and B is the perpendicular applied magnetic field density. Particles have their angles changed due to Lorentz force while interacting with the applied magnetic field. The Lorenz force serves as a constant centripetal force and the particles will travel circumferentially. The centripetal force of the circumferential movement of a moving particle can be expressed as

$$F_{\mathrm{e}} = mv^2/\rho, \tag{2}$$

where F_{e} is the centripetal force, m is the mass, and ρ is the bending radius. Let F equal to F_{e}, the equation obtained is

$$p = qB\rho, \tag{3}$$

where p is the momentum. For a relativistic electron,

$$E^2 = p^2c^2 + m_0^2c^4, \tag{4}$$

where E is the particle energy, c the velocity of light, and m_0 the rest mass. Substituting Eq. (3) into (4) yields the following relation between energy and circumferential radius

$$E^2 = (qB\rho)^2c^2 + m_0^2c^4. \tag{5}$$

In our energy measuring work, q takes on the value e, which is the electronic charge, and B can be computed from the geometric configuration of the magnetic analyzer and its supply voltage.

2.2   The image expansion

By crossing the uniform magnetic field, particles with different momenta would have their trajectories separated and hit on the target at different positions, as shown in Fig. 1. This helps to form dispersion lines or an energy spectrum. Therefore, compared with a single energy beam, a beam with an energy spread will have its spot image broadened.
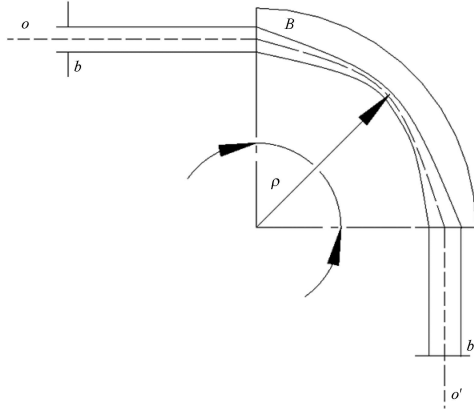

Fig. 1.   Beam energy differentiation.

For a magnetic analyzer with a specific characteristics, the image width is affected as follows.

(a) The slit width b, which is the width of the entry beam. In the specific magnetic field, only the particle at the speed v_0 will move on the reference orbit with the bending radius ρ. The image width b of the exit beam can be expressed as [6],

$$b' = Mb, \qquad (6)$$

where M is the magnification ratio, which is determined by the characteristic of the magnetic analyzer,

$$M = b'/b = -f/(1-g), \qquad (7)$$

where f is the focus of the magnetic analyzer, l is the distance of the object to the edge of the magnet, and g is the distance of the focus to the edge of the magnet.

(b) The momentum of deviating electron, which can be expressed as

$$v_r = (v - v_0)/v_0. \qquad (8)$$

For electrons with a relativity momentum v_r, the image width b' can be expressed as

$$b' = \rho v_r (1-M). \qquad (9)$$

The image width in total is a sum of the two parts

$$b' = Mb + \rho v_r (1-M). \qquad (10)$$

According to the relationship between momentum and energy, we know that the energy spectrum is

$$\varepsilon = \Delta E/E = \Delta p/p = v_r, \qquad (11)$$

so Eq. (8) can be rewritten as

$$b' = Mb + \rho \varepsilon (1-M). \qquad (12)$$

For measurement convenience, the full width of the slit is often adopted instead of b as

$$w = 2b, \ w' = 2b'. \qquad (13)$$

The energy spread can be expressed as

$$\varepsilon = 4w'/\rho(1-M). \qquad (14)$$

By measuring the image width w', we can calculate the energy spread.

2.3   Three-dimensional emulator result

The designed magnet was optimized with the 3D static field module Tosca of the Opera program, which is developed by Vector Fields Co. Ltd. [7]. The structure of the magnet was finely revised so that the calculated magnetic field distribution along the orbit center, as shown in Fig. 2, could meet the demand for precision.
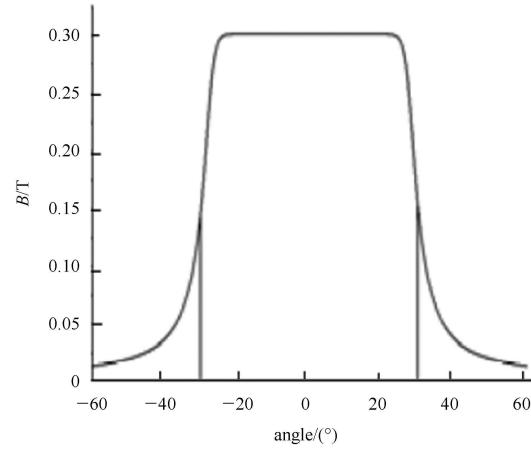

Fig. 2.   Distribution of B on the center orbit.

The calculated magnetic field along the radius around 300 mm is shown in Fig. 3. The designed magnet, which is characterized by broad distribution of fringe field and rotation angle of 60° with hard-edge approximation, is fairly consistent with the design expectation. Fig. 4 shows that the good field region is broad and the width of the good field region along the radius is about 65.4 cm (from $r=267.2$ mm to $r=332.6$ mm), with an adopted tolerance of 1%. Fig. 5 reveals the magnetic field distribution at radii of 270 mm, 300 mm, and 330 mm, which coincides with each other within the hard-edge of the magnet.

The calculated excitation curve, shown in Fig. 6, is linearly dependent on an excitation current below 4 A. The excitation current in common use is about 3 A, which lies in the mentioned linear region at low current and contributes considerably to experimental convenience.
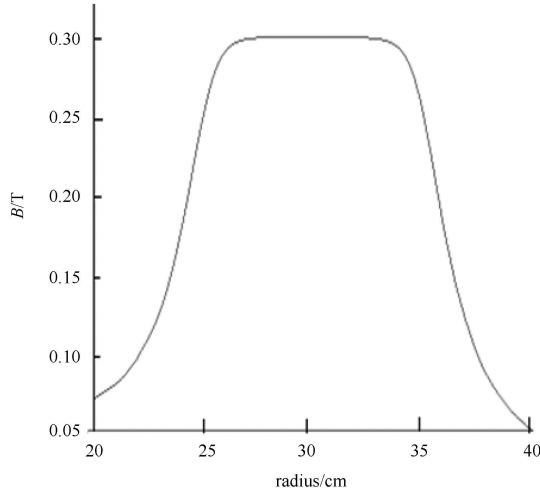

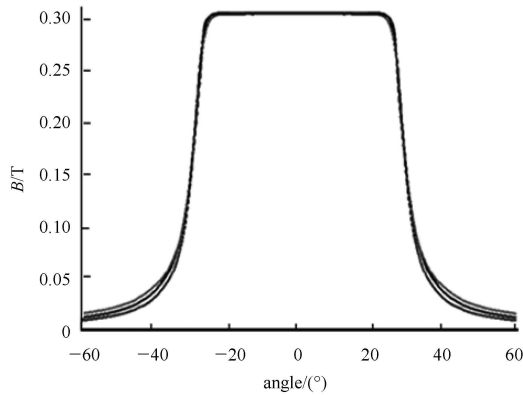Fig. 3.   Distribution of B on the radius.

Fig. 4.   Distribution of B on different orbits.
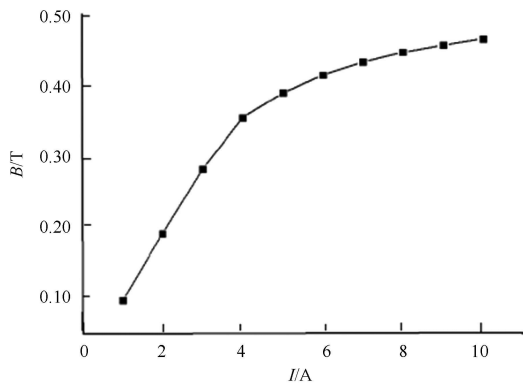

Fig. 5.   Linearity of the magnetic exciting.

According to experience, the effective length of the dipole magnet is larger than the physical length in a hard-edge approximation case: $\Delta l \approx (1.05 \sim 1.15)\delta$, δ is the magnetic gap. 3D simulation corresponds to theoretical design perfectly taking $\delta=1.10$ if the magnet edge is not beveled. In the case of a non-beveling design, the field concentration at the sharp corner would induce the saturation and limit the performance of the magnet on the acute angle effect. Our simulation result shows that saturation could be effectively restrained with beveling: the maximum field at magnet corner would be reduced from 2.245 T to 1.672 T, which is quite close to the linear region of DT4, if the magnet is only beveled for 3 mm.

3   Experimental setup

The experimental layout, shown in Fig. 6, is composed of a drift tube, a magnetic analyzer, and a detector on the beam line. As an electron bending element, the magnetic analyzer with a 300 mm-bending radius and a 60° bending angle is constructed on the beam line. The electron beam, within the restriction of a slit at the entrance, passes through the analyzer, interacts with the quartz glass target at the exit, and generates optical light, which provides both position and size information. The optic spot is recorded by the multi-frame gated synchronization monitor module.

The drift spaces that are located both upstream and downstream of the magnetic analyzer are 52 mm long. The slit is 0.5 mm wide.
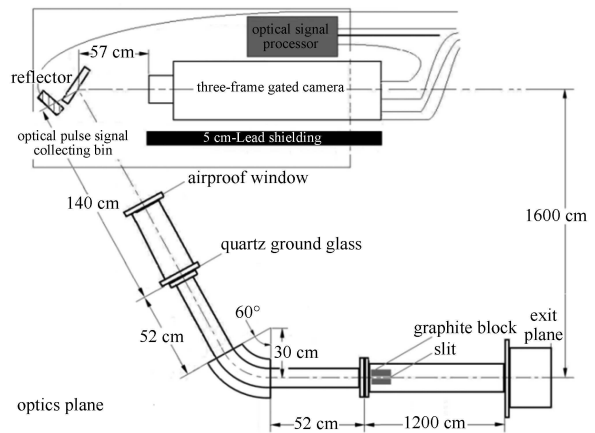

Fig. 6.   The energy measurement setup.

The magnetic analyzer is supplied with a constant current of 10^{-3} A and it runs at a field of around 0.02 T. The exact value is measured with a flux meter.

Within the whole system, shown in Fig. 7, the framing camera is part and parcel.

The time and space resolving power and imaging dynamic range are important measures of its performance. Intensifier Charge Coupled Device (ICCD) is the key part

of the camera, as is shown in Table 1. It is typically composed of a micro channel plank (MCP), a coupling lens, and a CCD camera. A high-speed MCP [8, 9] with a 25 mm cathode diameter and 2 ns shutter time is utilized as an image gating part.
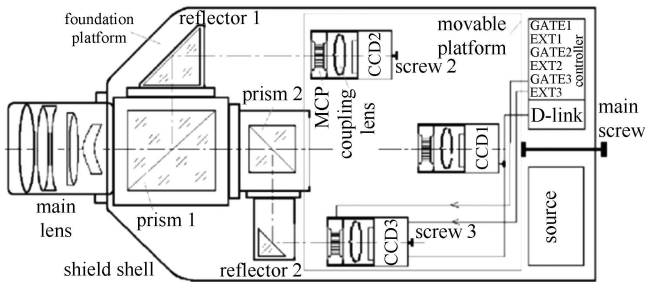

Fig. 7.   The structure of a framing camera.

Table 1.   Main performance of three-frame gated ICCD.

parameters	min	max	step
exposure time/ns	2	~109	<0.5
interval time/ns	~0	~109	<0.5
spatial resolution/(p.mm)		>30	
equivalent background lamination (EBL)			
(electrons·pixel·s)		10	
response uniformity		2%	
linearity		99%	
inherent insertion delay/ns	36.8	37.3	
image size in diameter/mm		25	

To work properly, usually two trigger inputs are needed; that is, one external trigger synchronization signal (EXT) and one image increase gating trigger signal (GATE). The synchronization signal is obtained by a pulse acquisition device in an accelerator cell, which will get the current pulse(or prepulse) loaded from pulse power system and pass it to the trigger equipment. Delayed for a certain time, the signal is utilized as the input of the multi-frame gated synchronization monitor module. After an inherence delay, the framing camera turns on its gate and begins to photograph. The image of the pulse electron beam falls into the gated duration of the camera by delay time [10, 11].

4   Results

Energy measurement experiments performed at the Dragon Accelerator have demonstrated the feasibility of using the time-resolved diagnostic system as a beam parameter measuring instrument.

Figure 8 shows online images of the beam spots captured in three 10 ns periods interspersed among the flat-topping part of the pulse with delay times of 130, 190, and 210 ns, respectively. The corresponding measured image widths are 1.96, 1.89, and 1.78 mm. Multiple experiments have indicated that the energy spread is $\Delta E/E \leqslant 2\%$.

Fig. 8.   Images of the beam spots captured with a 10 ns shutter.

5   Conclusion

The difficulty of measuring the magnetic field exactly and the beam orbit accurately have previously been a limit to their application in the measurement of beam energy. The time-resolved optical diagnostic system has greatly improved the accuracy of these measurements. The error mainly comes from the hard-edge approximation of the magnetic pole of the magnet and the circle arc simplification of the beam trajectory. The error from the edge-effect of the analyzer magnet is about 5%; the error from the aberration of beam orbit is about 3.5%. The total error in the energy measurement is less that 10%. For the energy spread, with an error about 3.5% from the data reading out of the image slit, the total error is less than 12%, although the nonlinear relationship between energy E and magnetic field B makes it difficult to determine the exact level.

References

1 DENG J J, CHEN S F, LI J et al. High Power Laser and Particle Beams, 2003, **15**(7): 705–707 (in Chinese)
2 JIANG X G, WANG Y, ZHANG K Z et al. High Power Laser and Particle Beams. 2012, **24**(5): 101–104 (in Chinese)
3 WANG Y, XIE Y T, CHEN S F et al. High Power Laser and Particle Beams. 2012, **24**(4): 950–952
4 WANG Y, JIANG X G, YANG L B et al. Scientia Sinica Techologica, 2011, **41**(12): 1580–1583
5 WEI-Kai Yu. Theory of Electrification Beam Transmission. Beijing: Science Press, 1986
6 YE-Ming Han et al. The Static Accelerator. Beijing: Science Press, 1965
7 Vector Fields Limited. Opera-3D User Guide. Vector Fields Limited, UK, 2008
8 JIANG X G, WANG Y, YANG G J et al. High Power Laser and Particle Beams, 2013, **25**(11): 2780–2784 (in Chinese)
9 WANG Y, JIANG X G, YANG G J et al. High Power Laser and Particle Beams, 2006, **15**(1): 101–104 (in Chinese)
10 JIANG Xiao-Guo, LI Cheng-Gang, WANG Yuan et al. High Energy Physics and Nuclear Physics, 2006, **30**(8): 784–787 (in Chinese)
11 WANG Y, JIANG X G, CHEN S F et al. High Power Laser and Particle Beams, 2014, **26**(4): 043201